EUROPEAN ORGANIZATION FOR NUCLEAR RESEARCH
ORGANISATION EUROPEENNE POUR LA RECHERCHE NUCLEAIRE

CERN - PS DIVISION

PS/ BD/ Note 99-15

ION CURTAIN PROFILOMETER

J. Bosser, E. Chevallay, C. Dimopoulou, A. Feschenko*, R. Maccaferri

*Present address: INR-Moscow

Geneva, Switzerland
9 November 1999

1) Introduction

The aim of this detector is to measure the transverse distribution of particle beams of small dimension and great density.

The principle on which the detector is based has been reported in reference [1]. It relies on the deflection of a low-energy ion-pencil-beam when passing perpendicularly through a dense particle beam. In the present paper the probed beam consists of protons. The proof of principle has been reported in reference [2], after experiments made on the CERN-SPS beam.

In the conclusions of [2] it was proposed to use a thin ion-curtain probe (or test) beam, instead of the ion-pencil beam, so as to avoid the scanning technique. Complementary to the ion-curtain method, a variant, so called "shadow" technique, has also been proposed [2, 3].

This paper reports the tests and measurements made with the "ion-curtain", on the SPS beam. After a brief recall of the principle, a summary of the results will be given and commented on.

In order to not make this paper too exhaustive, the technical description, involving the ion gun itself, will be left out. However mention will be made of the possible use of such an ion profilometer on the CERN-Linac, Booster and PS machines.

2) Data - Symbols

2.1 Data

$q = 1.6 \times 10^{-19}$ C , elementary charge,

$\varepsilon_0 = 8.854\times10^{-12}$ F m^{-1}, vacuum permittivity, $\dfrac{1}{4\pi\varepsilon_0} = 8.987\times10^{9}$ F^{-1} m,

$c = 2.997\times10^{8}$ m s^{-1}, velocity of light,

$m_p = 1.672\times10^{-27}$ kg, proton mass.

2.2 Symbols used for the ion probe beam

Nominal velocity : v_0 [m s^{-1}]

A, Z Atomic mass and charge, $m_i = A\, m_p$, $Q = Z\, q$ (Z = 1 in the present case)

$E_k = \frac{1}{2} A\, m_p\, v_0^2$ nominal kinetic energy

2.3 Symbols used for the probed proton beam ($A_p = 1$, $Z_p = 1$)

$\beta_0 = \frac{v_{proton}}{c}$

r.m.s bunch length : Δ_s [m], $L_b \equiv \Delta_s \sqrt{2\pi}$, $\sigma_t \equiv \frac{L_b}{\beta_0 \cdot c}$ [s]

r.m.s transverse dimensions : σ_x and σ_y [m], $\Delta_r = [\sigma_x^2 + \sigma_y^2]^{1/2}$

For round beams : $\sigma_x = \sigma_y = \sigma \Rightarrow \Delta_r = \sqrt{2}\ \sigma$

n_b ≡ number of protons / bunch

$V_o = \frac{q}{4\pi\varepsilon_0} \frac{2n_b}{L_b}$ [Volt]

T[s] time interval between bunches

3) Principle (Fig.1.a, 1.b)

The system of co-ordinates is defined in Figure 1.a, whilst the detector principle is recalled in Figure 1.b.

A low energy ion pencil beam is generated at : ($x = -x_i$, $y = y_0 \leq |x_i|$, $z = 0$) and moves with initial velocity $\vec{v_i} = v_0\, \vec{e_x}$ perpendicular to the direction of the proton beam. The proton beam itself, centred at (0,0,0) moves with velocity $\vec{v_p} = \beta_0\, c\, \vec{e_z}$.

The proton beam is supposed to be very dense and has a transverse distribution function with r.m.s values σ_x and σ_y. For simplicity we suppose a round Gaussian beam so that the normalised transverse distribution is given by :

$$n_{\perp}(r) = \frac{2}{2\pi\Delta_r^{\,2}}\, exp\,(-\frac{r^2}{\Delta_r^{\,2}}) \quad , \quad r = (x^2+y^2)^{1/2} \qquad (1)$$

The restriction to a round beam does not affect the detector accuracy [2] .

In the case of a bunched proton beam, with time interval T between bunches, the protons are supposed to be relativistic ($\beta_0 \cong 1$) so that the electrical space charge field of the p-bunch is mainly radial $\overrightarrow{E_r} = E_r \overrightarrow{e_r}$. The relativistic condition is not absolutely necessary [2] but will be considered as being fulfilled in this paper.

On its way from $-x_i$ to x_f, where the detector is placed, the ion beam will be deflected, by an angle $\theta(y_0)$, as a result of the transverse proton space charge electrical field $\overrightarrow{E_r}$. For each impact parameter y_0 the detector in the observer plane ($x = x_f = L$, defined by $\overrightarrow{e_y}$ and $\overrightarrow{e_z}$) will record a spot at $Y=Y_0 = y_o + L\,\theta(y)$ when the p-beam is ON and at $Y = y_0$ when the p-beam is OFF. Then the deflection angle $\theta(y_0)$ can be obtained by :

$$tg\theta(y_0) \cong \theta(y_0) = \frac{Y_0 - y_0}{L}$$

It has been showed ([1] , [2] and appendix 1) that with minor simplifications the deviation angle can be expressed by :

$$\theta(y_0) = \frac{QV_0}{2E_k}\,\pi\, erf\left(\frac{y_0}{\Delta_r}\right) = \theta_{max}\, erf\left(\frac{y_0}{\Delta_r}\right) \qquad a)$$

with $\theta_{max} = \frac{QV_0}{2E_k}\,\pi$ [rad] and $erf(u) = \frac{2}{\sqrt{\pi}}\int_0^u e^{-\xi^2} d\xi$ the error function; $erf(\infty) = 1$, $erf(0) = 0$, $erf(x) = -erf(-x)$ (2)

$$\text{Then : } \frac{d\theta(y_0)}{dy_0} = \frac{2\cdot\theta_{max}}{\sqrt{\pi}\cdot\Delta_r}\; e^{-\frac{y_0^2}{\Delta_r^2}} \qquad b)$$

$$\text{and so } \Delta_r = \frac{2\cdot\theta_{max}}{\sqrt{\pi}}\;\frac{1}{d\theta/dy_0|y_0 \to 0} \qquad c)$$

A plot of $\theta(y)$ (y here means y_0) , defined by 2.a, is given in Figure 2 for two different values of θ_{max} , namely for $\theta_{max} = 5\times10^{-3}$ rad (curve $\theta1$(y)) and for $\theta_{max} = 10\times10^{-3}$ rad (curve $\theta2$(y))

whilst $\Delta_r = 10^{-3}$ m for both cases. Figure 3 represents equation 2.b for both values of θ_{max} and for the given Δ_r.

Once 2.b is evaluated a normalisation is applied, namely $\left(\frac{1}{2\cdot\theta_{max}}\right)\cdot\frac{d\theta(y_0)}{dy_0}=\frac{1}{\sqrt{\pi}\cdot\Delta_r}\cdot e^{-\frac{y_0^2}{\Delta_r^2}}$ which is the is equivalent in y (or y_0) direction of equation (1) and therefore represents the distribution, we intend to retrieve from our measurements.

Conclusions

Having measured $\theta(y_0)$, one can deduce θ_{max} and $d\theta(y_0)/dy_0$ (equation 2.b). The later equation is, according to (1), representative of the density distribution in the proton bunch in the y direction. The radial r.m.s value Δ_r can then be obtained from 2.c. However, we found this method of data treatment to be not very precise, because important errors are induced during the numerical derivation of $\theta(y_0)$. It can therefore be used only for rough estimates.

In practice, after having measured the deviation angle θ as a function of y_0 (or y), we proceed with an "erf-fit" of the measured data. The fit gives the optimal value Δ_r. Then we compute $\frac{\partial\theta_{fit}}{\partial y_0}$ so as to obtain the bunch distribution in the y direction.

Remark : In the case where $\sigma_t / T < 1$ a modulation of θ_{max} with time occurs [2]. This effect is quite small and therefore negligible in the present case where we use heavy probe ions.

4) Ion curtain beam [2]

If, instead of scanning the ion beam in the y direction we use a flat inclined curtain ion source, the measurement becomes as described by Figure 4.

The ions forming the curtain are produced from a source situated on the x axis upstream of the probed beam ; each ion has therefore a velocity component in the x direction and one in yz plane . The geometry between the ion source and the observer plane is explained in detail in Appendix 3 .

For simplicity, in order to avoid heavy and complicated notations, we will consider throughout the paper that the ions forming the curtain move in the x direction. (In other words we will consider the ion source to be very far away from the probed beam so that the y,z velocity components of the ions are negligible.) Of course, during the experimental measurements and the data treatment we took into account the real geometry described in Appendix 3 .

The thin ion beam is distributed along the line $y = z.tg(\varphi)$. When the proton beam is OFF, the corresponding line is directly recorded on the observer screen orthogonal to the ion direction at $x = x_f = L$.

When the proton beam in ON, the ion at ordinate y is deflected by an angle $\theta(y)$ and reaches the observer plane at $Y = y + L\, tg\theta = y + L\, \theta(y)$.

After some linear transformations we retrieve the distribution $\theta(y)$ in a similar way as explained in paragraph 3.

Again an "erf-fit" is applied on the measured values (see paragraph 3) from which we deduce the p-bunch density distribution, in the y direction, and thus Δ_r.

This method dispenses with scanning and is independent of the ion curtain density $dn_i / d\xi$ (Fig. 4) . The determination of the bunch centre of gravity is immediate.

The essential part of this paper concerns measurements made on the CERN-SPS with such an inclined ion curtain.

4.1) Shadow technique

A variant has been proposed [3], namely the so called "Shadow" technique. It makes use of the same arrangement. The principle is the following : With proton-bunch OFF the probe ion lies on the 0Y line of the observer plane with density

$$\frac{dn_i}{dY} = \frac{dn_i}{dy}$$

$\frac{dn_i}{dy}$ being determined by the ion source properties.

When the proton-bunch is ON a measurement of the ion density gives,

since $Y = y + L\theta(y) \equiv g(y)$:

$$\frac{dn_i}{dY} = \frac{dn_i}{dy}\,\frac{dy}{dY} = \left(\frac{dn_i}{dy}\right)\frac{d}{dY}\left(g^{-1}(Y)\right)$$

The interpretation of the measurements is not straightforward (see appendix 2), since $\frac{dn_i}{dy}$ is not constant and also since θ_{max}, which appears in the derivative $\frac{d}{dY}\left(g^{-1}(Y)\right)$ depends on n_b and therefore on the proton beam intensity.

In order to implement this technique it would be preferable to have an ion curtain lying in the xy plane, that is with $\varphi = \pi/2$ .Then 2-dimensional resolution is not needed and one could avoid the use of a camera and the subsequent image treatment. A 1-dimensional detector with the proper resolution in the y direction (for example strips, fibres) could be used instead. However, $\varphi = \pi/2$ is not a mandatory condition; on physical grounds the choice of φ is of no importance. In our experiment $\varphi = \frac{\pi}{10} \neq \frac{\pi}{2}$ (Fig. 4) and the shadowing effect was observed. This will be briefly reported.

5) Ion curtain profilometer set-up

The schematic set-up is given in Figure 5. The gun (Ion source-Extractor-Drift tube) itself consists in an industrial ion source which has been modified and used with Xe^+ during all the experiments. The outcoming ion beam has a conical distribution and is steered toward a small aperture slit. The part of beam not traversing the slit hits a collector plate. The beam coming out of the slits is focused so to form the required thin ion curtain when crossing the proton beam.

After being deflected by the proton beam space-charge electric field the ions are amplified (by a Micro-Channel-Plate) and produce photons on a phosphor screen.

The resulting image is viewed with a Vidicon type camera having a fixed resolution of 625 points in Z and, due to the band-width of 5MHz, an equivalent of 540 points in Y. The Vidicon analogue signal is then digitised by means of an appropriate Data Acquisition card which can give a maximum of 576 pixels in Z and 768 pixels in Y. The useful part of the digitised image corresponds to 440 pixels in Z and 350 pixels in Y. The resolution therefore depends on the performance of the Data Acquisition Card. There are more performant cards

than the one we used; in addition, Vidicons with larger band-widths are available. Higher resolution can therefore be achieved. We note that our aim up to now has been to test the physical principle of the profilometer and not to provide a performant operational diagnostic.

Care has been taken to ensure a small vacuum pressure increase inside (10^{-8}torr) in the vacuum pipe. Vacuum valves insures, when necessary, a full seperation of the detector from the machine.

6) SPS machine parameters

The SPS operated in fixed target mode with the following parameters :

- Total number of protons : 1.8×10^{13} - 2.4×10^{13}
- Number of bunches : 4200
- Number of protons per bunch $n_b = 4.3\times10^9 - 5.7\times10^9$
- r.m.s bunch duration 0.5ns
- time interval between bunches $T \cong 5$ns
- revolution frequency 44 kHz
- momentum versus time

$$p(t) \cong 14 + 0.1253\ (t\text{-}1260)(\text{ms})\ \text{GeV/c}$$

where t refers to the first injection.

The detector was installed at location IWS41432 near a wire scanner used as reference (location 41420). The machine parameters at the IWS level are: $\beta_H = 94.61$ m,

$\beta_v = 22$ m, Dispersion $D_H = 2.83$ m.

7) Experimental measurements

One of the observations made with the Vidicon camera is shown in Figure 6. In the presence of the proton beam we can observe the "S" shaped ion curtain around the virtual inclined straight line measured when the proton beam is OFF.

A preliminary but essential work is to proceed with calibration and more precisely to determine the coefficients : Number of mm on the phosphor screen/ number of pixels in both directions Z and Y. These coefficients were p_z =0.164 mm/pixel and p_y =0.112 mm/pixel respectively .

The intersection between the straight line and the "S" shaped curve determines the "zero" point, or the proton beam centre of gravity.

After having measured the function $\theta(Y)$ one takes into account the geometrical parameters (L , D and $\varphi = \frac{\pi}{10}$) (Fig. 5) and finally obtains the function $\theta(y)$.

Using estimates (initial guess values) of θ_{max} and Δ_r we proceed with an "erf-function" fit to find the optimised θ_{max} and Δ_r .

The overall detector performances and the data treatment are of prime importance for acquiring accurate measurements.

A plot of θ_{max} as a function of the inverse ion kinetic energy is given in Fig. 7. The linearity is verified over almost all the range of interest.

8) Transverse r.m.s dimension

We made many measurements of the transverse beam dimension using different probe ion kinetic energies and comparing our measurements with those taken from the neighbouring wire-scanner.

Figure 8 shows a plot the transverse r.m.s value σ, as a function of pc [GeV], measured with the ion profilometer and with the wire-scanner. Results are quite comparable. The transverse r.m.s value σ decreases as expected.

Figures 9.a and 9.b represent the transverse profile expressed by equation 2.b normalised to 2 θ_{max} *(i.e.* $\left(\frac{1}{2\cdot\theta_{max}}\right)\cdot\frac{d\theta(y_0)}{dy_0} = \frac{1}{\sqrt{\pi}\cdot\Delta_r}\cdot e^{-\frac{y_0^2}{\Delta_r^2}}$ *)* for different proton beam energies during the SPS cycle. As mentioned before, the plotted curves are the derivatives made on the accurate "erf-fit". The area under each curve is equal to 1.

9) Error estimate in determining $\Delta_r = \sqrt{2}\,\sigma$

As showed in Fig.1.b an ion with impact parameter y_0 will reach the phosphor screen at

$Y = y_0$ when the proton beam is OFF
$Y = Y_0 = y_0 + L\,\theta(y_0)$ when the proton beam is ON

The phosphor screen is seen by a Vidicon type camera through an optical system (Fig. 10a). Therefore, after digitising the Vidicon signal, to the point :

A of ordinate $Y = 0$ [mm] corresponds the pixel number : P_A
B of ordinate $Y = y_0$ [mm] corresponds the pixel number : P_B
C of ordinate $Y = Y_0 = y_0 + L\,\theta(y_0)$ [mm] corresponds the pixel number : P_C

The overall range covered by y_0 corresponds to the use of one row of N pixels.

We have obtained a calibration factor p_y [mm/pixel].

For a given impact parameter y_0, the deviation angle $\theta\,(y_0)$ can be computed by (Fig.10.a).

$$\theta(y_0) = \frac{p_y}{L}\left[P_c(y_0) - P_B(y_0)\right]$$

As explained above, we then proceed with an erf-fit on the data so as to obtain the optimal Δ_r and θ_{max} :

$$\theta(y_0) = \theta_{max}\,\mathrm{erf}\left(\frac{y_0}{\Delta_r}\right) \quad , \quad \Delta_r = \sqrt{2}\,\sigma$$

In fact the probe ion pencil beam (or curtain) has a finite width (or diameter) so that it appears to be distributed over a few (8 – 10) pixels on the P axis representing the camera input. The treatment program seeks for the pixel number where the maximum light intensity occurs. The corresponding uncertainty is estimated to be δ = ½ pixel. The error made on the deviation angle is therefore independent of the impact parameter y_0.

$$\Delta\theta = 2\delta\,\frac{p_y}{L}$$

9.1) Error simulation procedure

a) From experimentally measured values θ_{max} and Δ , we consider a theoretical model

$$\theta\,(y_0) = \theta_{max}\,\mathrm{erf}\left(\frac{y_0}{\Delta}\right)$$

Due to pixelisation, the impact parameter y_0 takes discrete values namely (Fig. 10.b)

$$y_0 \equiv y_k = y_{min} + k\,\frac{y_{max} - y_{min}}{N}$$

y_{max} = + 7mm and y_{min} = -7mm are fixed. Therefore the theoretical distribution is given at discrete points $\theta\,(y_0) \rightarrow \theta(\,y_k)$.

b) On the latter function we superpose random numbers uniformly distributed in [- $\Delta\theta$, $\Delta\theta$] so as to simulate the errors induced by the uncertainty in determining the maximum amplitude pixel. More precisely, we consider :

$$\Phi(y_k) = \theta\,(y_k) + 2\,\delta\,\frac{p_y}{L}\,(2\,\gamma_k - 1)$$

where γ_k are random numbers uniformly distributed in [0,1]

c) Then Φ is fitted by a function : $u_0\,\mathrm{erf}\,(y_k/u_1)$ and the optimal parameters : $u_0 \equiv \theta_{maxfit}$ and $u_1 \equiv \Delta_{fit}$, are obtained from the fit.

d) The relative error is expressed by :

$$error = \frac{\left|\Delta_{fit} - \Delta\right|}{\Delta}$$

and is averaged over a few ($\approx$ 12) random number "runs"

e) For simplicity we have represented in Fig.10.a the case $\varphi = \pi/2$ which corresponds to a 1-dimensional image. In reality, the ion curtain is inclined by $\varphi = \pi/10$ with respect to the z axis (Fig. 4) which leads to a 2-dimensional image on the camera. Therefore, the overall range covered by y_0 corresponds to N pixels in z (and not in y) direction (Fig. 4), for which we have obtained the calibration coefficient p_z [mm/pixel]. We note that $p_z \neq p_y$.
Then obviously $N \propto 1/p_z$.

Results are given in table 1 for which it must be recalled that $\theta_{max,}$, Δ ,

p_z = 0.164 mm/pixel (which corresponds to N = 400) , p_y = 0.112 mm/pixel do actually concern our experiment.

Fig. 10.b shows the function $\Phi(y_k) = \theta_{max}\ \mathrm{erf}\left(\frac{y_k}{\Delta}\right) + 2\,\delta\,\frac{p_y}{L}\,(2\,\gamma_k - 1)\,)$ and the corresponding fit $\theta_{maxfit}\ \mathrm{erf}\,(y_k/\,\Delta_{fit})$ for the CASE *1a* (θ_{max} = 0.010 rad , Δ = 2.29 mm) and for the CASE *5a* (θ_{max} = 0.0028 rad , Δ = 2.33 mm) of Table 1.

Relative error estimates in determining $\Delta_r = \sqrt{2}\cdot\sigma$.

CASE	p_y (mm/pixel)	p_z (mm/pixel)	N	θ_{max} (rad)	Δ (mm)	Relative Error $\lvert\ \Delta_{fit}-\Delta\ \rvert / \Delta$
1a	0.112	0.164	400	0.010	2.29	4 %
1b	0.056	0.082	800	0.010	2.29	3 %
2a	0.112	0.164	400	0.0095	2.19	4.5 %
2b	0.056	0.082	800	0.0095	2.19	3.3 %
3a	0.112	0.164	400	0.0077	2.22	6 %
3b	0.056	0.082	800	0.0077	2.22	4.5 %
4a	0.112	0.164	400	0.0052	2.11	11 %
4b	0.056	0.082	800	0.0052	2.11	8.5 %
5a	0.112	0.164	400	0.0028	2.33	14 %
5b	0.056	0.082	800	0.0028	2.33	14 %

Table 1

9.2) Remarks

From Table 1 we conclude that

- For the same θ_{max} the relative error is less important when the digitisation is bigger (p_y smaller). This is expected since :

$\eta_k \equiv \Delta\theta\ (2\gamma_k\text{-}1) = 2\,\delta\,\frac{p_y}{L}\,(2\,\gamma_k - 1) \propto p_y$ and the number of points $N \propto 1 / p_z$.

- For fixed resolution the relative error decreases for higher θ_{max} values, that is for higher proton beam intensities and/or for lower probe ion beam energy.

This is also expected since for large θ_{max} the theoretical term $\theta_{max.}$ erf (y_k / Δ) is more important when compared to the random error term η_k .

- As far as the relative error is concerned, it is preferable to operate at low Xe^+ ion kinetic energies (1.5 –3 keV).

10) Shadowing technique

As explained in 4.1, and more detail in appendix 2, the shadowing technique makes use of the attenuation, induced by the proton bunch electrical field, on the ion probe-beam distribution. According to the simplified model described in Appendix 2, for a uniformly distributed ion probe-beam the "deflation" width on the phosphor screen should be about :

$2\,(2\Delta_r + L\,\theta_{max}(n_b))$.

Figure 11.a gives an example of the experimentally observed distribution. One should note that the data analysis was very tedious mainly because of difficulties in the smoothing techniques. As mentioned above, operation at $\varphi = \pi/2$ would make data treatment much more straightforward.

Figure 11.b presents the beam shadow results for different SPS proton beam momenta.

Figure 11.c shows the beam shadow results for a fixed proton beam momentum and for different θ_{max}. The value of θ_{max} was changed by varying the Xe^+ ions kinetic energy. The fact that some of the curves are shifted to the left is due to the smoothing algorithm and is of no importance for the interpretation of the results. One can see that the "deflation" width at fixed proton beam momentum and hence at fixed Δ_r depends on θ_{max} as expected (see Appendix 2).

11) Application to "low" energy machines

Studies have been made on the application of this type of detector on the other CERN machines namely Linac-2, PS-booster and PS [4].

Application to Linac-2 looks promising and would illustrate the case where proton beams are not fully relativistic (though still dense) since the beam energy is 50 MeV. The use of a curtain beam is then almost mandatory.

Concerning the Booster and the PS machine itself, the use of a scanned ion pencil beam could be considered instead.

12) Conclusions

The use of a thin inclined ion curtain, to measure a beam's transverse density distribution, has been investigated. The measurements made on the SPS gave valuable results, in accordance with theory. Making the ion curtain profilometer operational appears feasible, provided that more time and effort is dedicated to the improvement of the data treatment system.

The principle of shadowing the ion beam density has been demonstrated and needs further studies. This technique however does not give a straightforward measurement of σ since it involves the proton beam intensity (n_b) as well (see Appendix 2).

Of course both methods would allow to display the transverse profile all along the cycle every 20 to 40 ms.

13) Acknowledgements

We would like to thank the staff of the LHC vacuum group , SL-BI group and the SPS operation (namely G.Arduini) for their valuable help. This work was strongly supported by the LHC-ID committee.

REFERENCES

[1] Profilometer for small dimension proton beams.

J. Bosser, I. Meshkov.

PS/BD/Note 94-04 , CERN 1999 .

[2] Ion Profilometer for the SPS and LHC Accelerators.

J. Bosser, A. Feschenko, R. Maccaferri.

PS/BD/Note 99-07, CERN 1999.

[3] C.Bovet : private communication.

[4] Possible application of the ion profilometer for the Linac-2, PS-Booster and PS. J. Bosser, C. Dimopoulou, A. Feschenko, R. Maccaferri

(Unpublished note, CERN 1999)

FIGURE CAPTIONS

Figure 1: a) System of co-ordinates.

b) Symbols used and the principle of the ion pencil beam profilometer.

Figure 2: Plot of $\theta\,(y) = \theta_{max}\,\mathrm{erf}\left(\frac{y}{\Delta_r}\right)$ (equation 2a), as a function of y for $\Delta_r = 10^{-3}$m.

$\theta 1(y)$ corresponds to $\theta_{max} = 5\times10^{-3}$ rad and $\theta 2(y)$ corresponds to $\theta_{max} = 10\times10^{-3}$ rad.

Figure 3: Plot of $d\,\theta 1(y) / dy$ and $d\,\theta 2(y) / dy$ as a function of y. Again $\theta 1(y)$ corresponds to $\theta_{max} = 5\times10^{-3}$ rad and $\theta 2(y)$ corresponds to $\theta_{max} = 10\times10^{-3}$ rad and $\Delta_r = 10^{-3}$m .

Figure 4: Principle of the inclined curtain ion beam profilometer.

Figure 5: Ion curtain detector set-up. Top : Ion gun + Optics; Bottom : Overall set-up including the detector.

Figure 6.a: Image from the Vidicon camera of the ion curtain detector showing the ion curtain deformation due to proton bunches space-charge.

Figure 7: Plot of θ_{max} [rad] as a function of the inverse of the probe ions kinetic energy [keV].

Figure 8: Measurements of the horizontal r.m.s dimension σ [mm] as a function of the SPS beam momentum. Measurements are made with :

- The Xe^+ ion curtain at 1.81 keV and 2.72 keV kinetic energy. The relative error in determining σ was 6% for 1.81 keV ions and 11% for 2.72 keV ions.
- The wire scanner using raw and fitted data.

Figures 9.a , 9.b: Transverse beam profile, as a function of SPS beam momentum.

The plotted curves are the derivatives made on the accurate "erf-fit".

By normalisation it is meant that we plot :

$$\left(\frac{1}{2\cdot\theta_{max}}\right)\cdot\frac{d\theta(y_0)}{dy_0}=\frac{1}{\sqrt{\pi}\cdot\Delta_r}\cdot e^{-\frac{y_0^2}{\Delta_r^2}}.$$

The area enclosed by each curve is equal to 1.

Figure 9.a : measurements made with Xe^+ ions of 2.72 keV.

The relative error in determining σ was 11% .

Figure 9.b : measurements made with Xe^+ ions of 1.81 keV .

The relative error in determining σ was 4.5% .

Figures 10.a, 10.b : Error estimate in determining $\Delta_r = \sqrt{2}\,\sigma$.

Figure 10.a : Principle of error estimate and symbols used.
Figure 10.b : Results of the error simulation procedure for the CASE *1a* (θ_{max} = 0.010 rad , Δ = 2.29 mm) and for the CASE *5a* (θ_{max} = 0.0028 rad , Δ = 2.33 mm) of Table 1.
The function $\Phi(y_k) = \theta_{max}\,\mathrm{erf}\left(\frac{y_k}{\Delta}\right)+2\,\delta\,\frac{p_y}{L}\,(2\,\gamma_k - 1)\,)$ and the corresponding fit $\theta_{maxfit}\,\mathrm{erf}\,(y_k/\Delta_{fit})$ are shown for each case.

Figures 11.a ,11.b, 11.c: Shadow technique .

Figure 11.a : Example of the experimentally observed distribution .

Figure 11.b : Beam shadow results for different SPS proton beam momenta.

Figure 11.c : Beam shadow results for a fixed proton beam momentum and for different θ_{max}. The value of θ_{max} was changed by varying the Xe^+ ions kinetic energy.

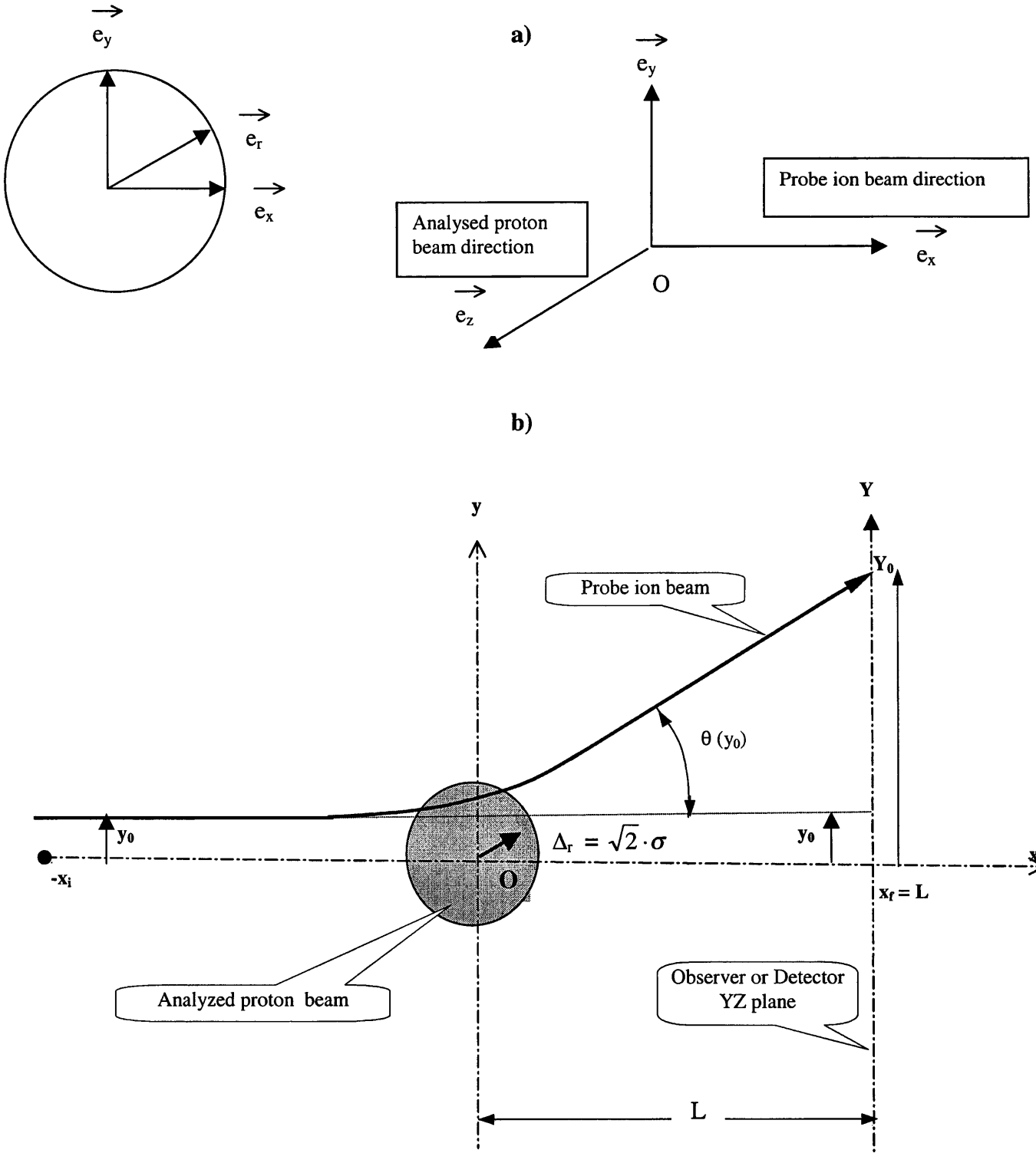
a)
e_y
e_r
e_x
e_y
Probe ion beam direction
Analysed proton beam direction
e_x
O
e_z
b)
y
Y
Y_0
Probe ion beam
θ (y_0)
y_0
$\Delta_r = \sqrt{2} \cdot \sigma$
y_0
x
$-x_i$
O
$x_f = L$
Analyzed proton beam
Observer or Detector
YZ plane
L

Figure 1

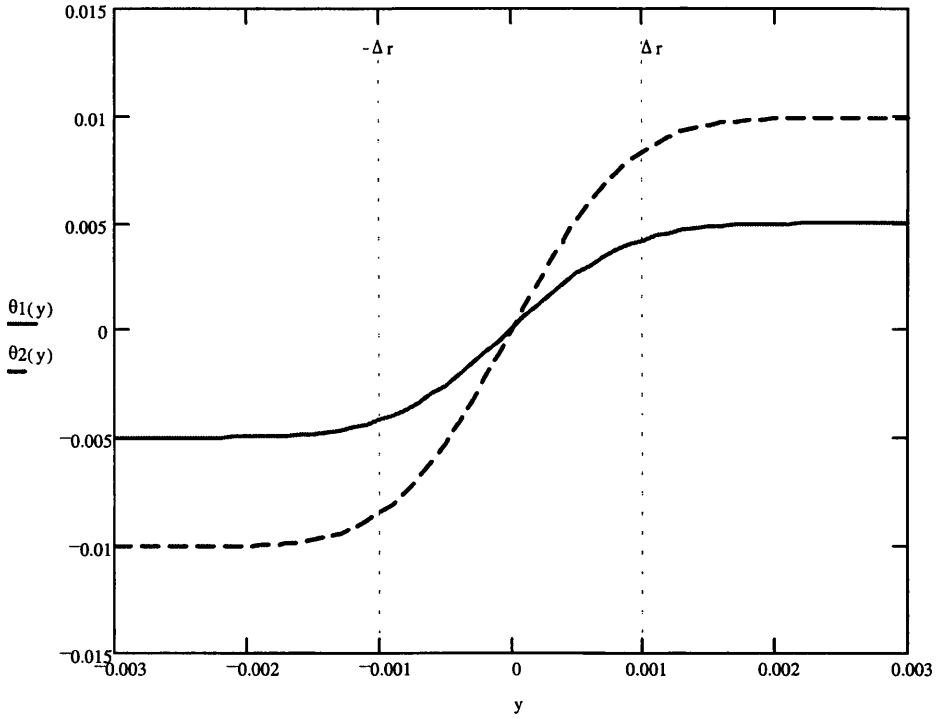

Figure 2

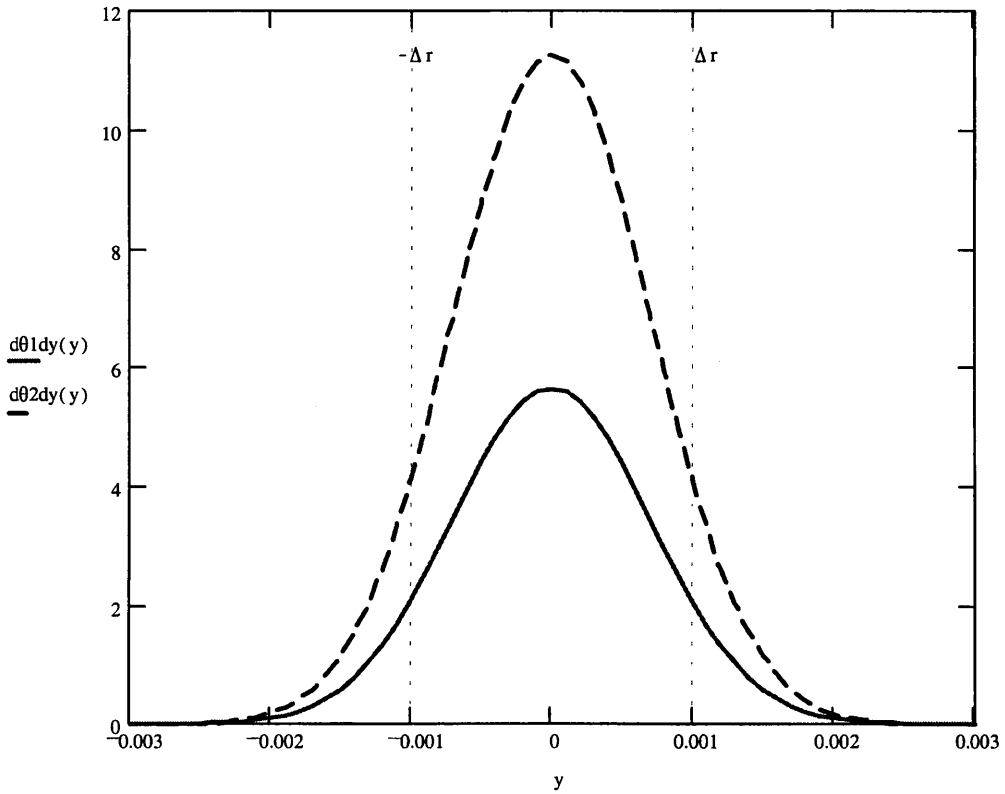

Figure 3

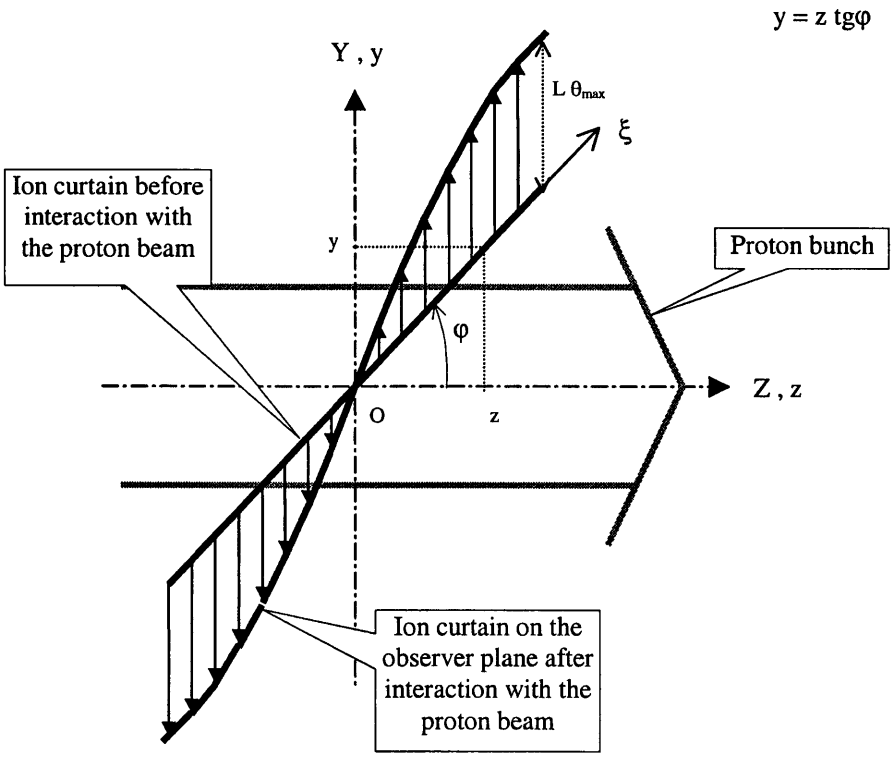
y = z tgφ
Y , y
L θmax
ξ
Ion curtain before interaction with the proton beam
y
Proton bunch
φ
Z , z
O
z
Ion curtain on the observer plane after interaction with the proton beam

Figure 4

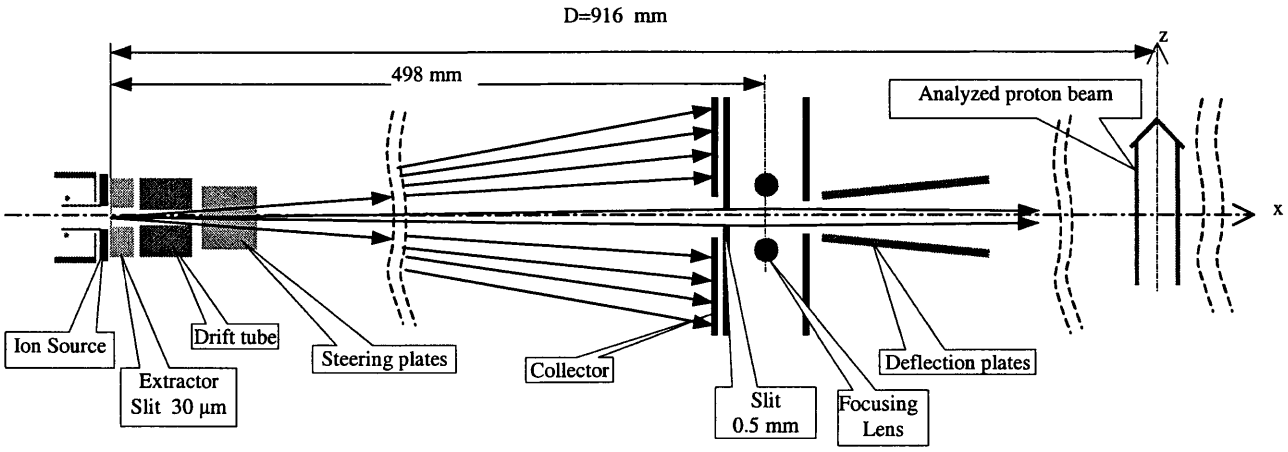
D=916 mm
498 mm
z
x
Analyzed proton beam
Ion Source
Drift tube
Steering plates
Collector
Deflection plates
Extractor
Slit 30 μm
Slit
0.5 mm
Focusing
Lens

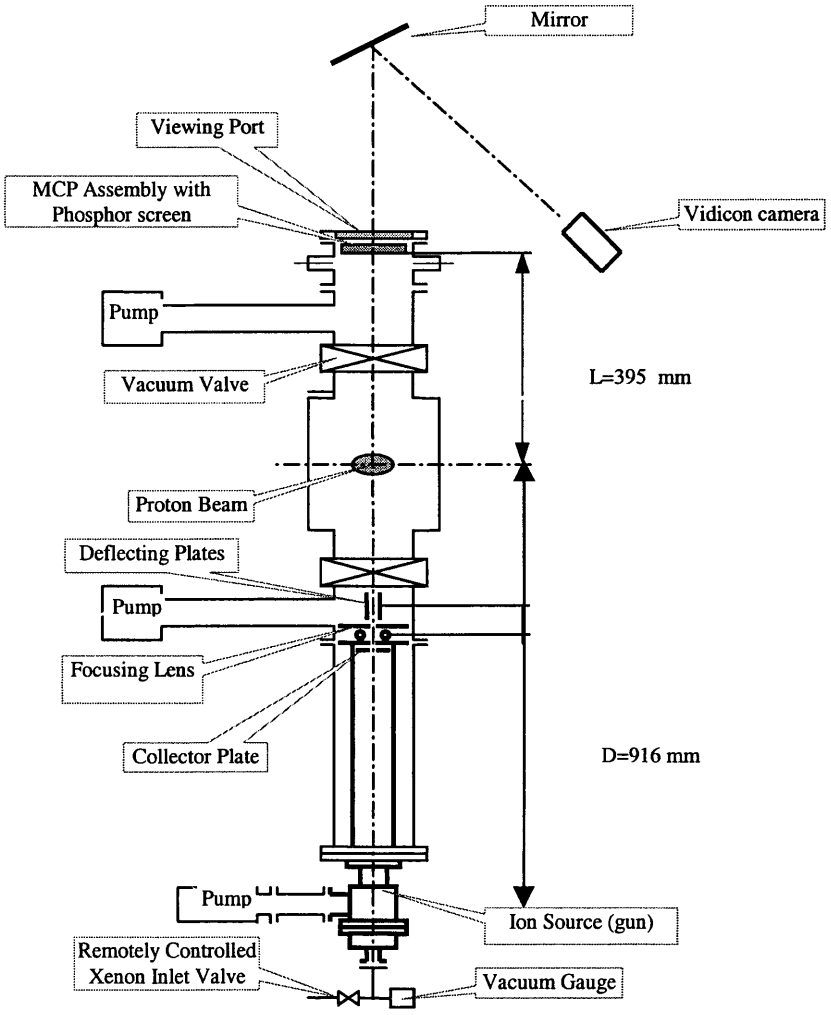
Mirror
Viewing Port
MCP Assembly with
Phosphor screen
Vidicon camera
Pump
Vacuum Valve
L=395 mm
Proton Beam
Deflecting Plates
Pump
Focusing Lens
Collector Plate
D=916 mm
Pump
Ion Source (gun)
Remotely Controlled
Xenon Inlet Valve
Vacuum Gauge

Figure 5

ION PROFILOMETER

Nominal (fixed target) SPS proton beam , intensity = 1.8×10^{13} protons

Xe^{+} ions energy : 2.72 keV

3500 ms from injection , proton momentum = 314 GeV/c

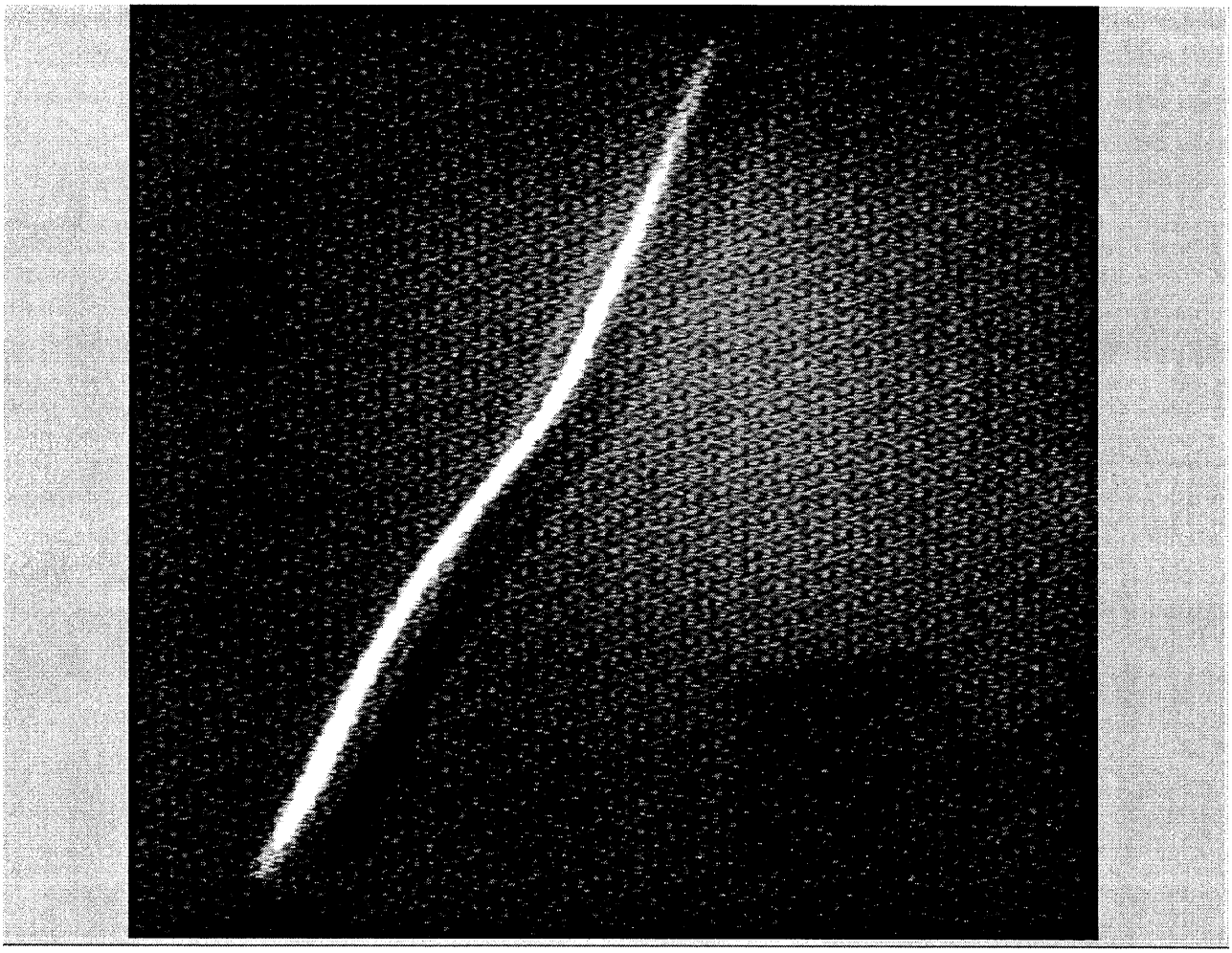

Figure 6

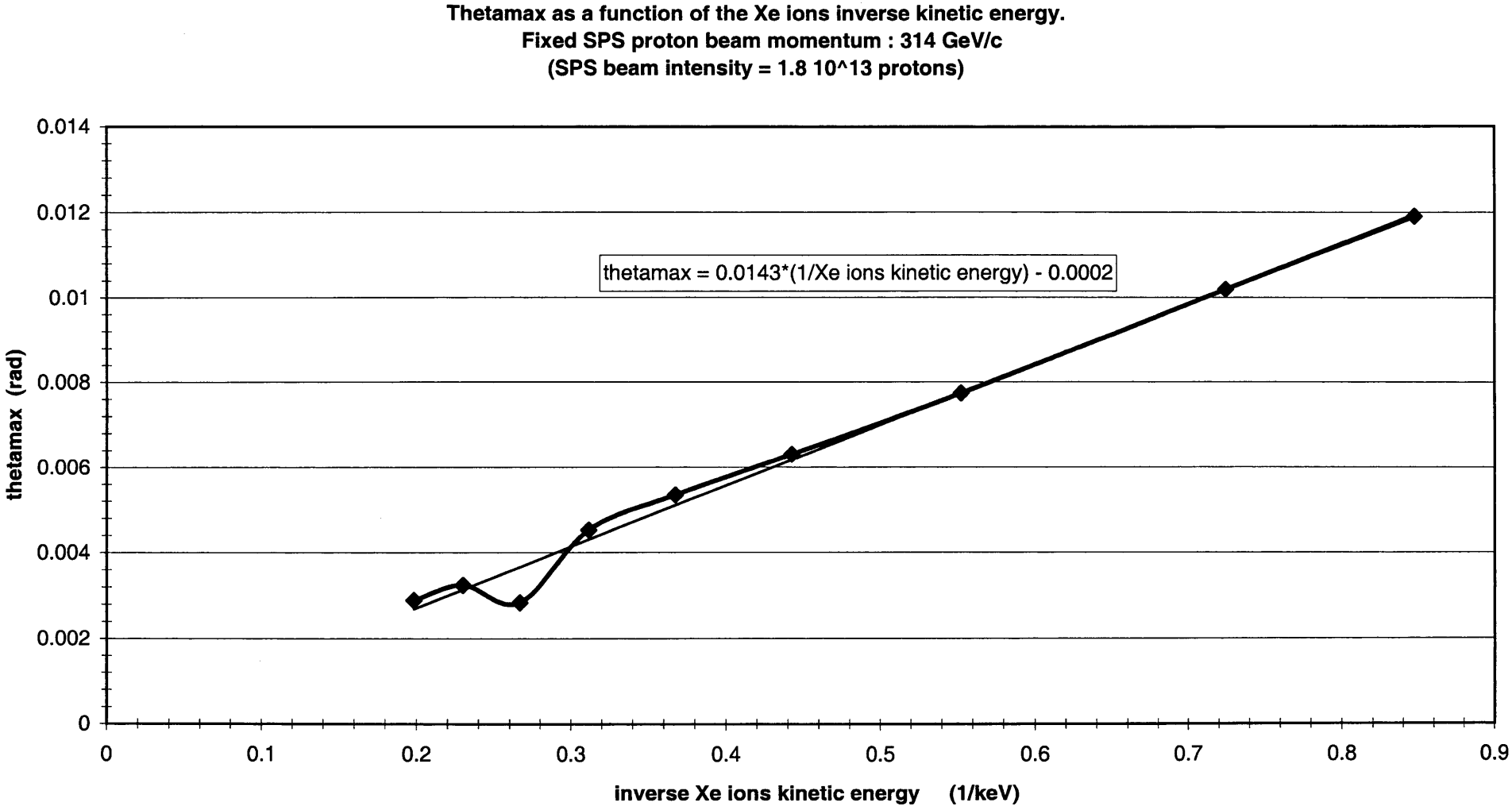
Thetamax as a function of the Xe ions inverse kinetic energy.
Fixed SPS proton beam momentum : 314 GeV/c
(SPS beam intensity = 1.8 10^13 protons)
thetamax = 0.0143*(1/Xe ions kinetic energy) - 0.0002
thetamax (rad)
0.014
0.012
0.01
0.008
0.006
0.004
0.002
0
0
0.1
0.2
0.3
0.4
0.5
0.6
0.7
0.8
0.9
inverse Xe ions kinetic energy (1/keV)

Figure 7

Evolution of proton beam horizontal r.m.s dimension (sigma) as a function of the SPS proton beam momentum: ion profilometer results for 2 different Xe ion energies and Wire Scanner results. (SPS beam intensity = 1.8 10^13 protons)

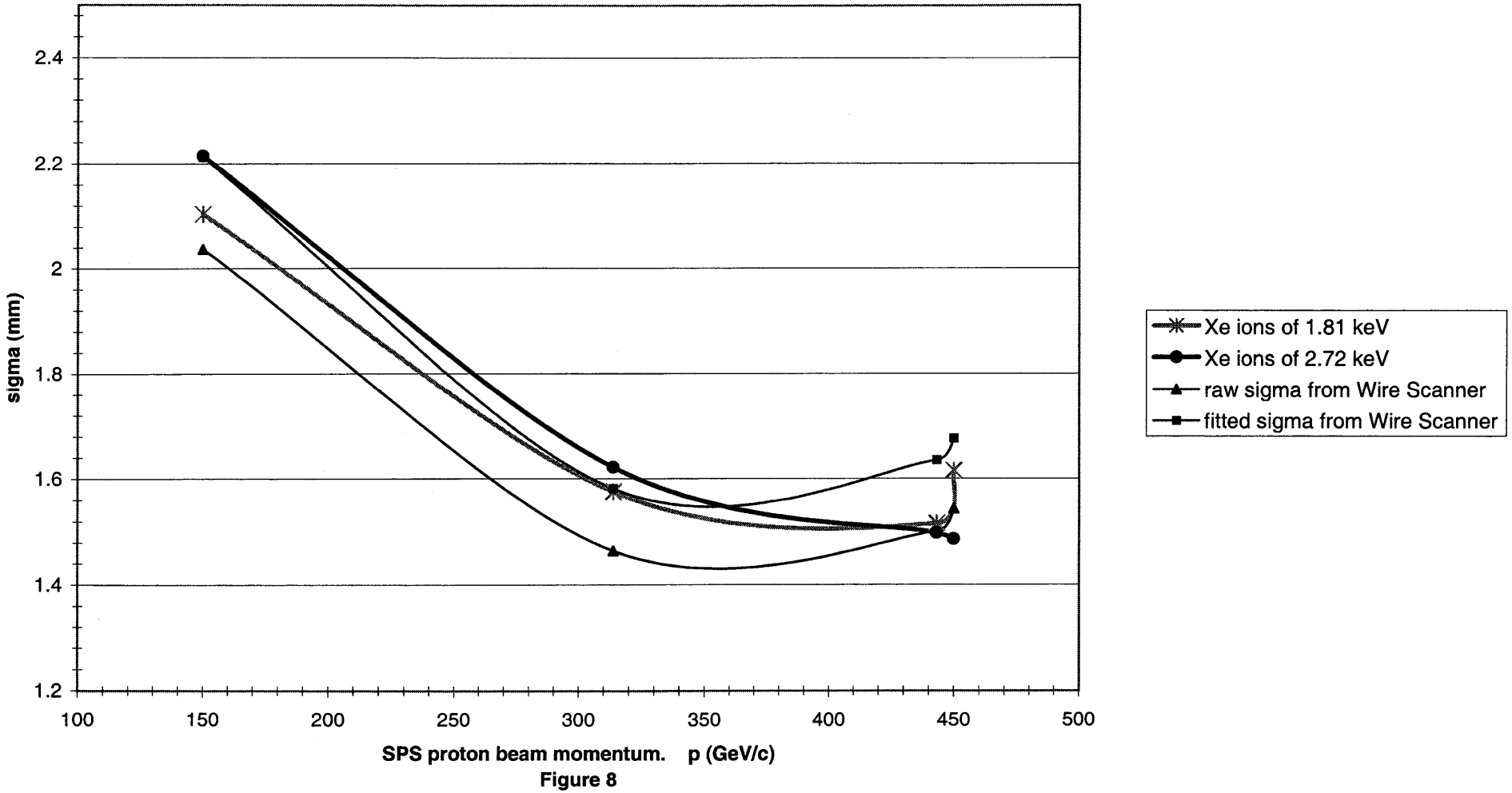

Figure 8

Normalised Horizontal Profiles of the SPS proton beam for different momenta during the SPS Supercycle.
The corresponding horizontal r.m.s dimension (sigma) is given as well.
Xe ions kinetic energy : 2.72 keV
(SPS beam intensity = 1.8 10^13 protons)

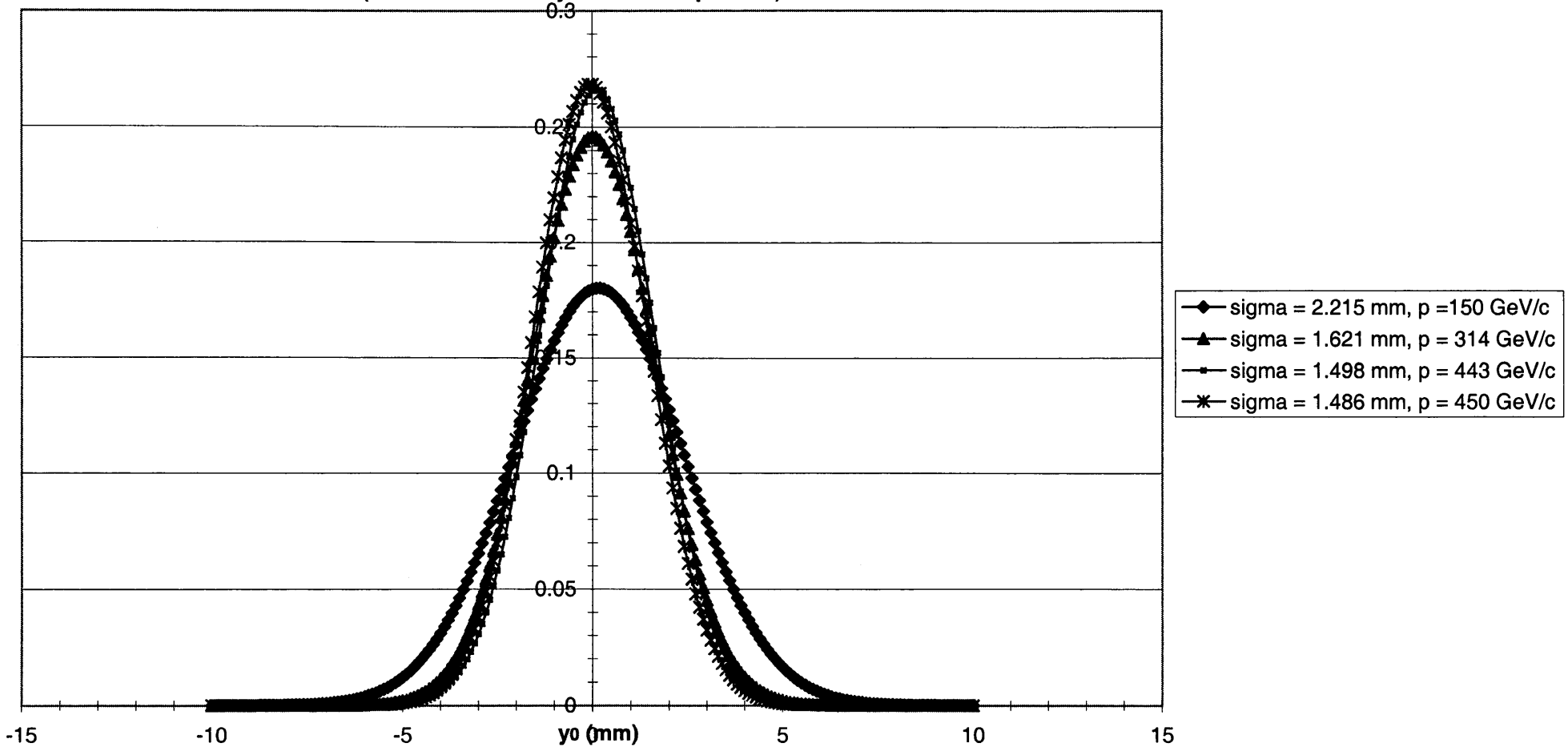

Figure 9.a

Normalised Horizontal Profiles of the SPS proton beam for different momenta during the SPS Supercycle.
The corresponding horizontal r.m.s dimension (sigma) is given as well.
Xe ions kinetic energy : 1.81 keV
(SPS beam intensity = 2.4 10^13 protons)

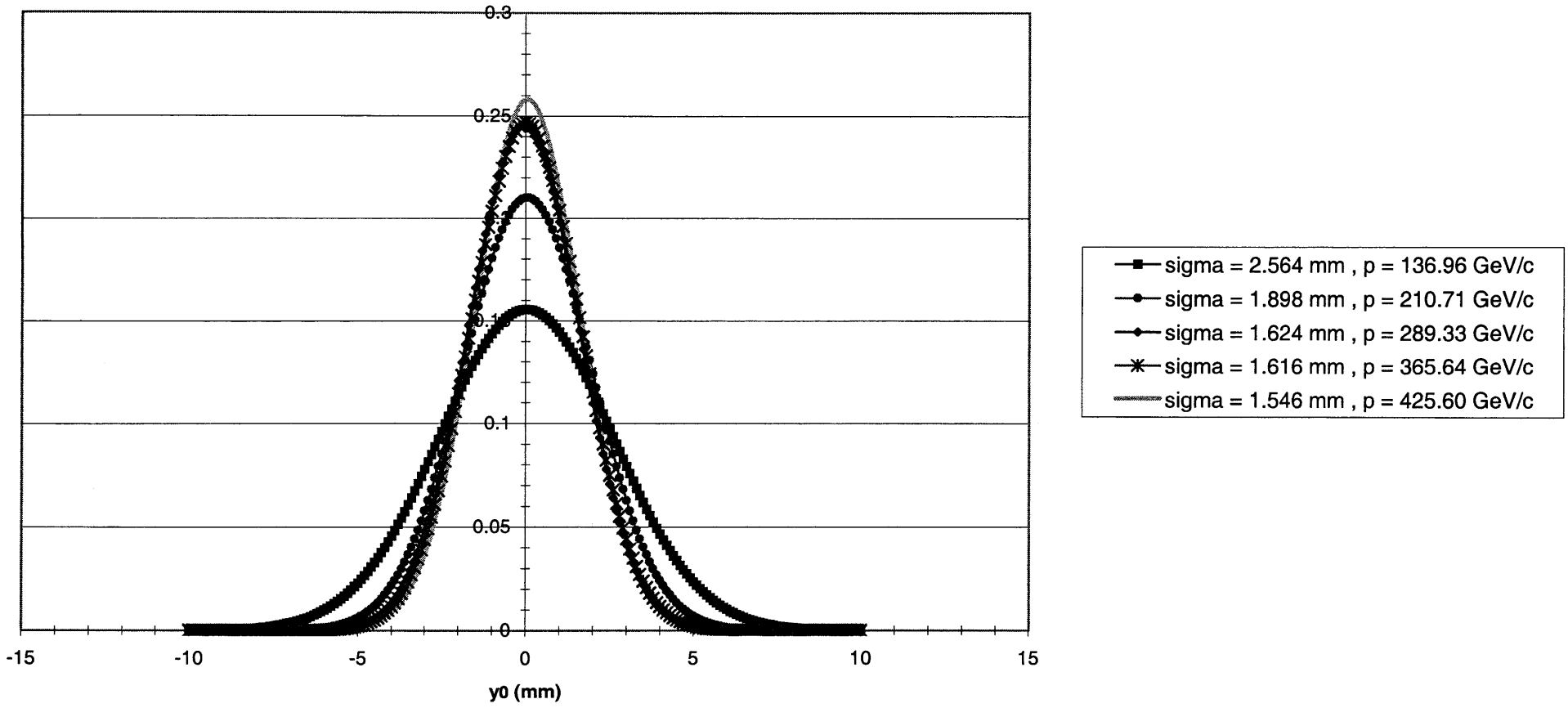

Figure 9.b

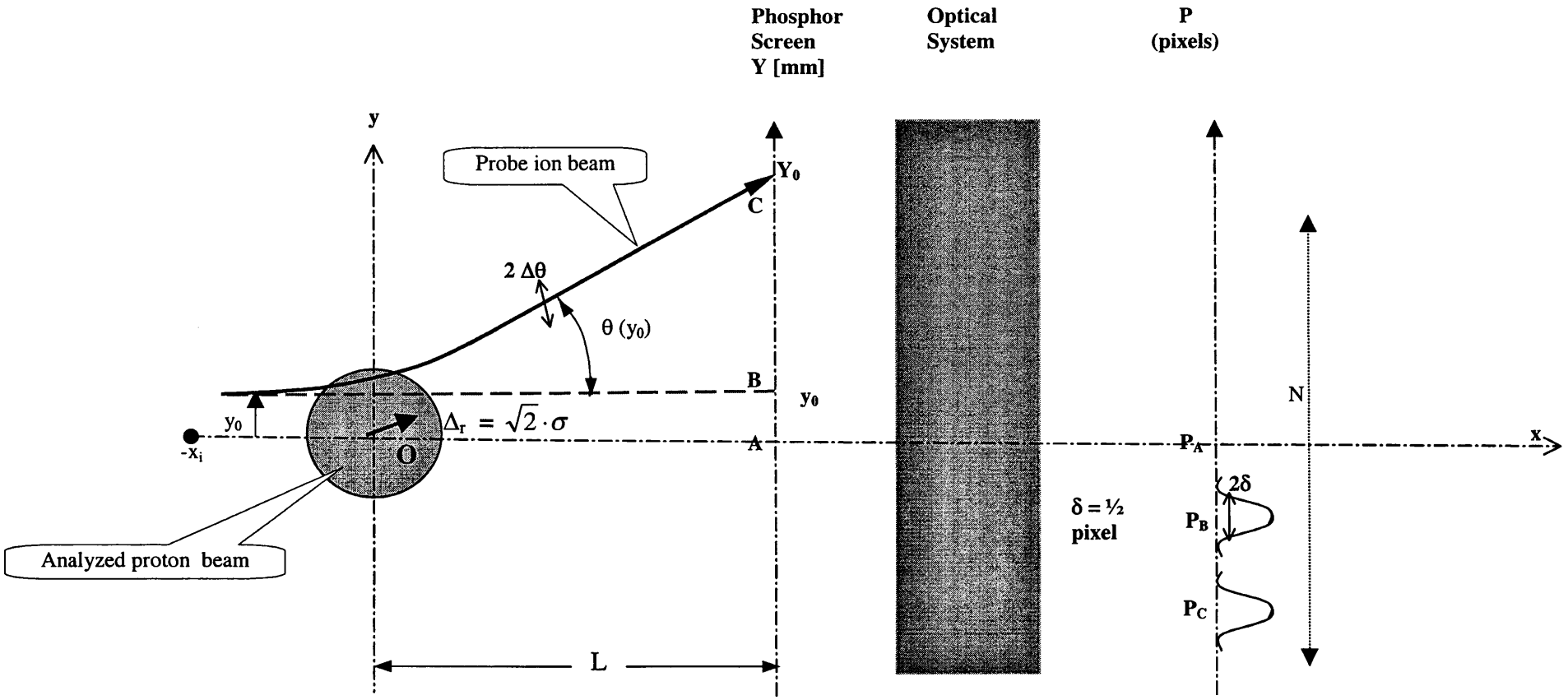
Phosphor
Screen
Y [mm]
Optical
System
P
(pixels)
y
Probe ion beam
Y_0
C
$2\Delta\theta$
$\theta(y_0)$
B
y_0
y_0
$\Delta_r = \sqrt{2}\cdot\sigma$
$-x_i$
O
A
P_A
x
N
2δ
$\delta = ½$
pixel
P_B
P_C
Analyzed proton beam
L

Figure 10.a

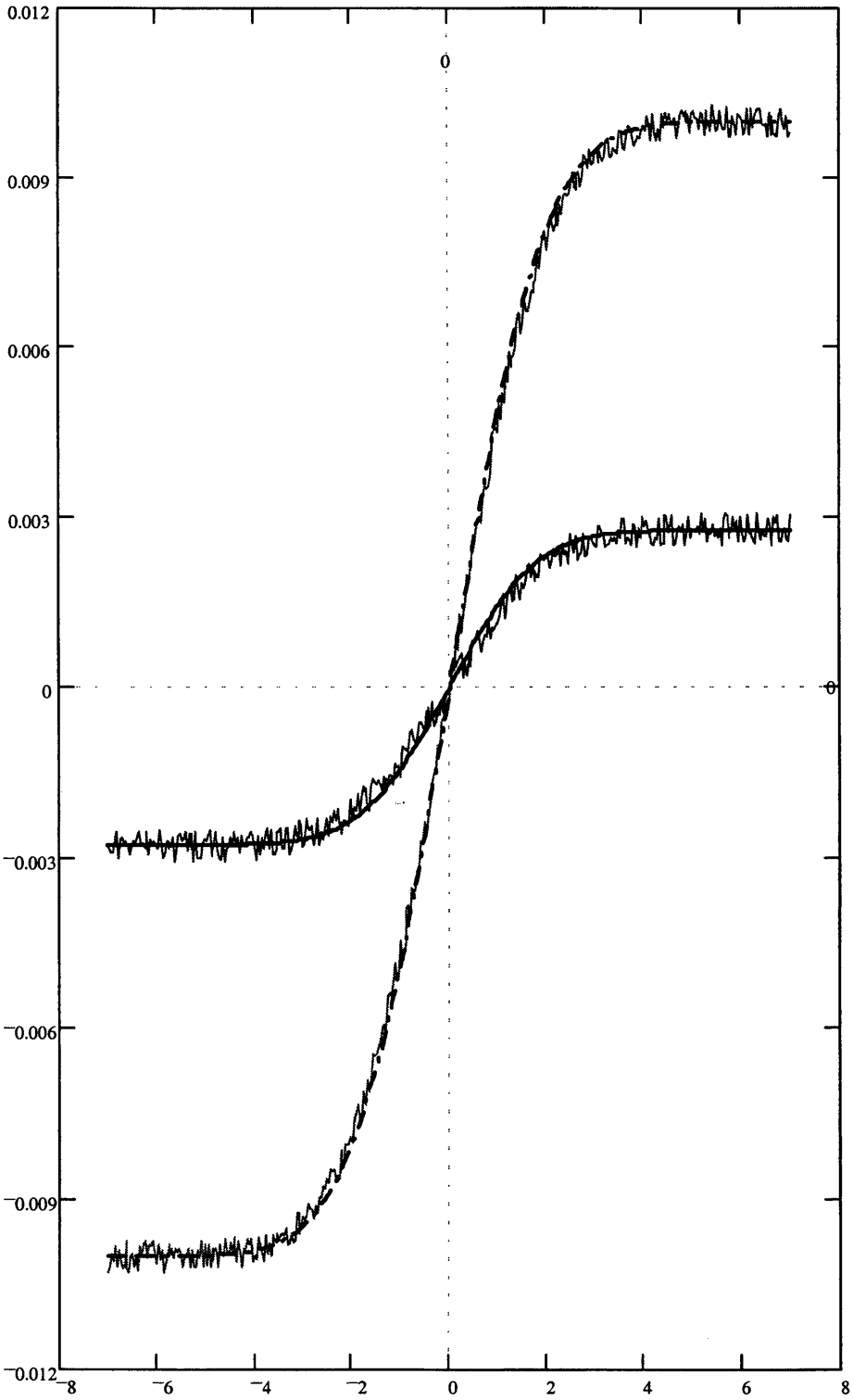

Figure 10.b

Example of raw shadow data.
Xe ion kinetic energy = 2.72 keV
SPS proton beam momentum p = 314 GeV/c
(SPS beam intensity = 1.8 10^13 protons)

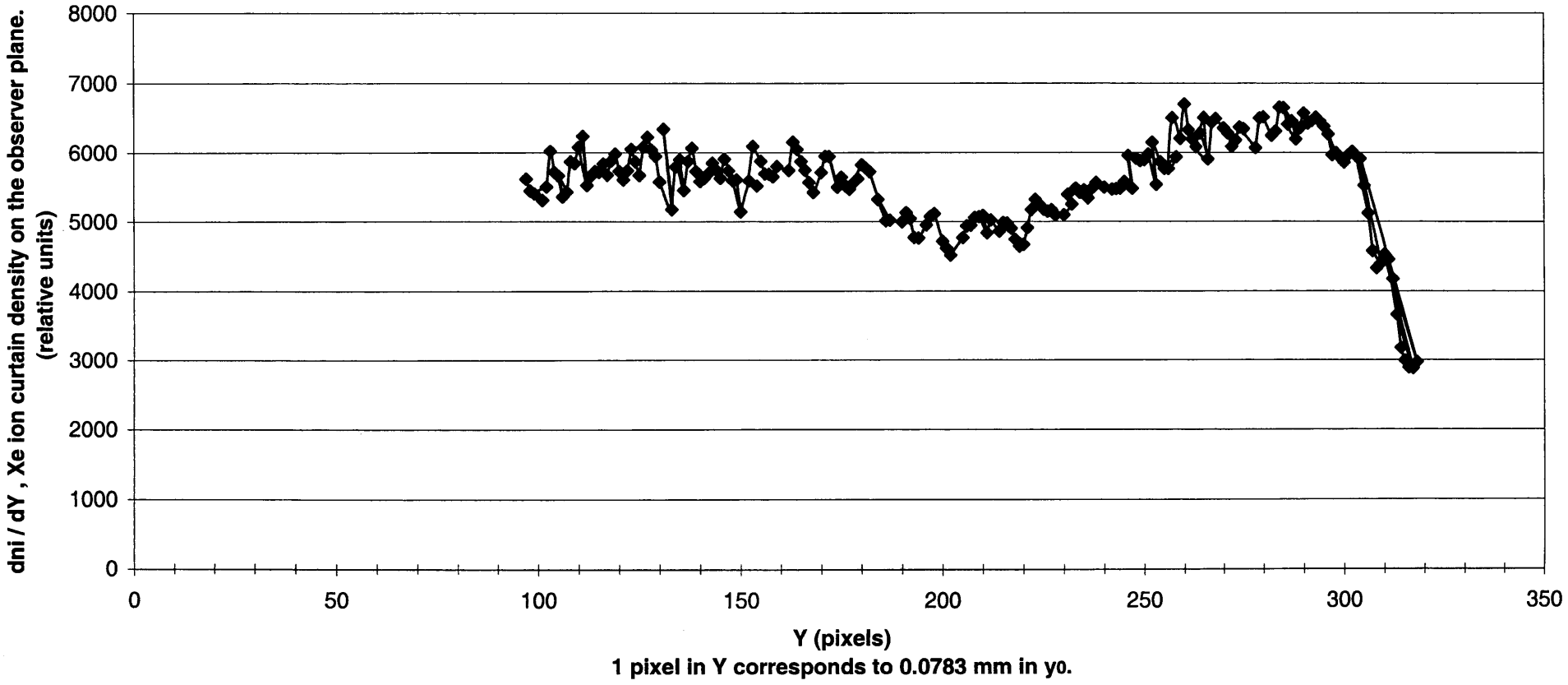

Figure 11.a

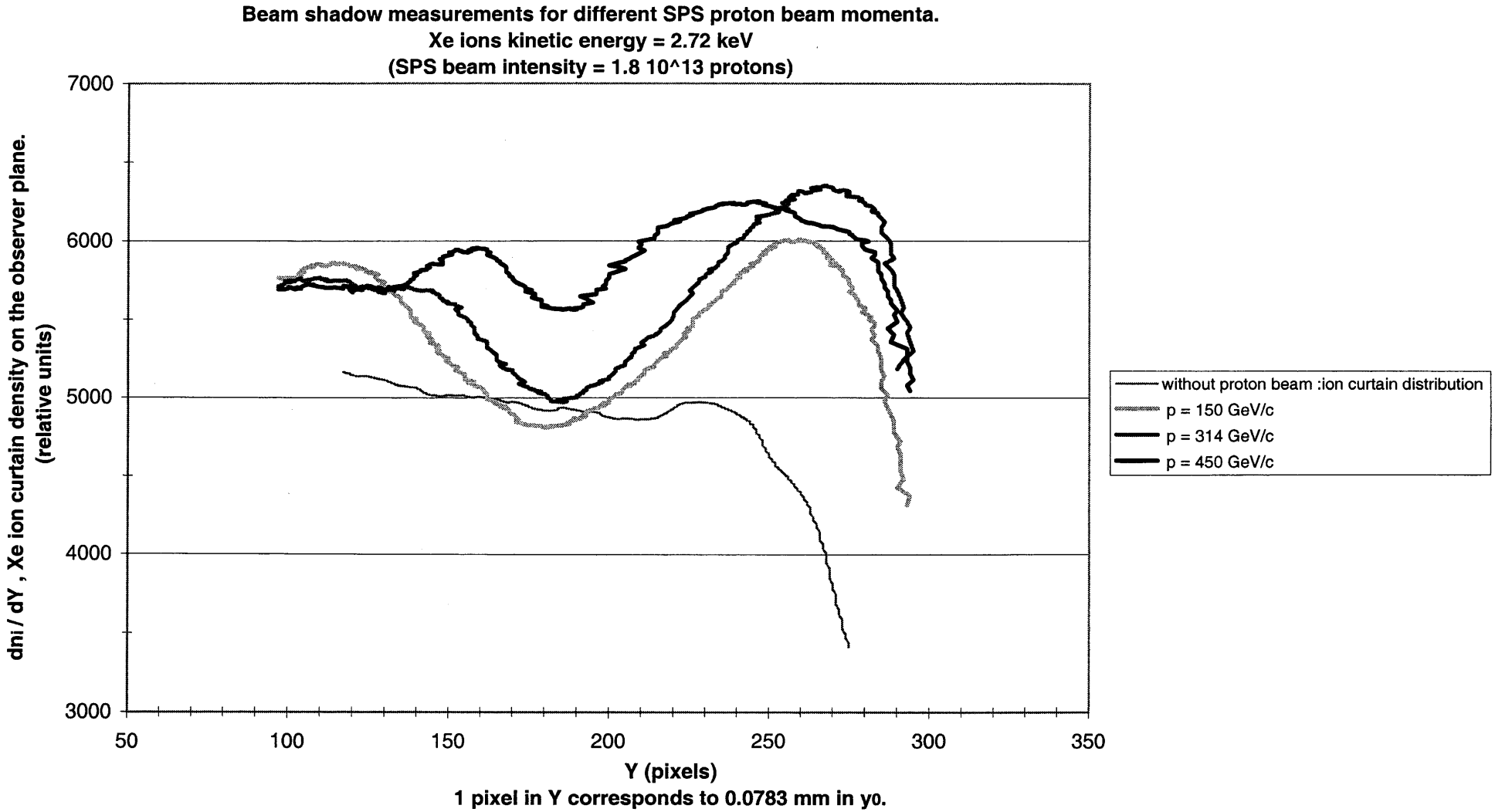
Beam shadow measurements for different SPS proton beam momenta.
Xe ions kinetic energy = 2.72 keV
(SPS beam intensity = 1.8 10^13 protons)
dni / dY , Xe ion curtain density on the observer plane.
(relative units)
7000
6000
5000
4000
3000
50
100
150
200
250
300
350
Y (pixels)
1 pixel in Y corresponds to 0.0783 mm in y0.
without proton beam :ion curtain distribution
p = 150 GeV/c
p = 314 GeV/c
p = 450 GeV/c

Figure 11.b

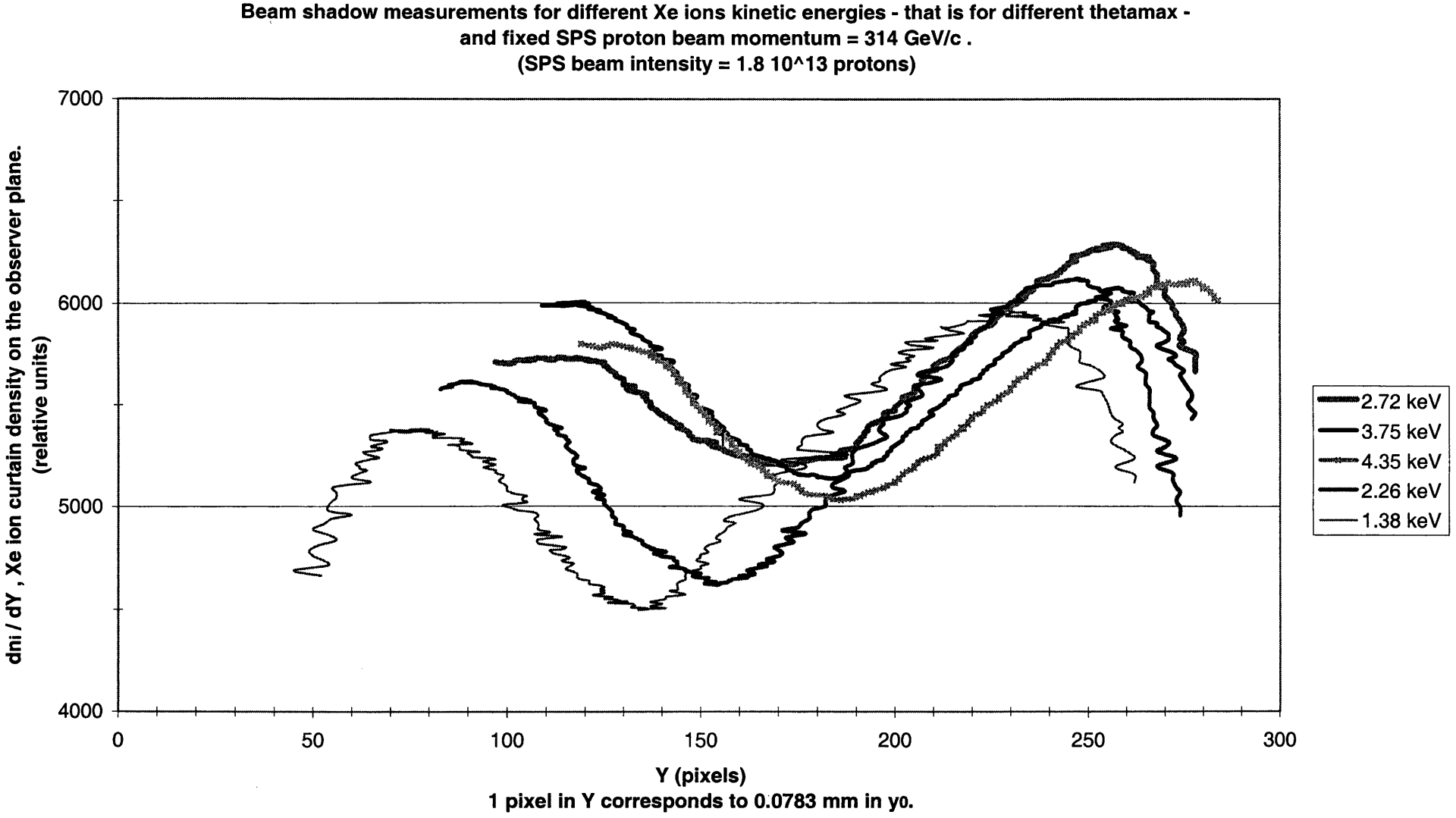
Beam shadow measurements for different Xe ions kinetic energies - that is for different thetamax -
and fixed SPS proton beam momentum = 314 GeV/c .
(SPS beam intensity = 1.8 10^13 protons)
dni / dY , Xe ion curtain density on the observer plane.
(relative units)
7000
6000
5000
4000
0
50
100
150
200
250
300
Y (pixels)
1 pixel in Y corresponds to 0.0783 mm in y0.
2.72 keV
3.75 keV
4.35 keV
2.26 keV
1.38 keV

Figure 11.c

APPENDIX 1

We aim to demonstrate that the deviation angle θ (y_0) can be, under some assumptions, approximated by an erf function.

A) Hypothesis

We consider a proton bunch having

- a transverse normalised distribution

$$n_\perp(r) = \frac{2}{2\pi\Delta_r^{\,2}}\ exp\,(-\frac{r^2}{\Delta_r^{\,2}}) \qquad r = \sqrt{x^2+y^2}$$

with r.m.s value : $\left(\int_0^\infty r^2 n_1(r) 2\pi r dr\right)^{1/2} = \Delta_r$

- an uniform longitudinal distribution over the length $L_b = \sqrt{2\pi}\ \Delta_s$

$$n_\sigma(z) = 1/L_b$$

So that the overall distribution is :

$$n(r) = \frac{1}{L_b} \cdot \frac{2}{2\pi\Delta_r^{\,2}}\ exp\,(-\frac{r^2}{\Delta_r^{\,2}}) \qquad (1)$$

where $n_b \equiv$ number of protons/bunch

B) Deflection angle as a function of the impact parameter y_0

It has been shown [1] that (Fig. 1)

$$\theta(y_0) = \frac{QV_0}{2E_k} \int_{-u_i}^{u_f} \frac{1 - e^{-\frac{y_0^2}{\Delta_r^2}(1+u^2)}}{1+u^2}\, du \qquad (2)$$

$u \equiv x/y_0$, $u_f \equiv x_f/\Delta_r >> 1$, $u_i \equiv x_i/\Delta_r >> 1$ where the symbols are those defined in paragraph «Symbols». Differentiating :

$$\frac{d\theta(y_0)}{dy_0} = \frac{QV_0}{2E_k}\ \frac{2y_0}{\Delta_r{}^2}\ e^{-\frac{y_0{}^2}{\Delta_r{}^2}} \int_{-u_i}^{u_f} e^{-\left(\frac{uy_0}{\Delta_r}\right)^2}\ du$$

and for $u_f, u_i \rightarrow \infty$ a good approximation will be

$$\left(\frac{d\theta(y_0)}{dy_0}\right)_{approx} = \frac{QV_0}{2E_k} \cdot \frac{2\sqrt{\pi}}{\Delta_r}\ e^{-\frac{y_0{}^2}{\Delta_r{}^2}} \qquad (3)$$

C) Error function

It is well known that

$$\text{erf}(u) \equiv \frac{2}{\sqrt{\pi}} \int_0^u e^{-\xi^2}\, d\xi\,, \qquad \frac{d(erf(u))}{du} = \frac{2}{\sqrt{\pi}}\, e^{-u^2},$$

erf(0) = 0, erf(∞) = 1, erf(x) = -erf(-x).

Applied to (3) gives an approximate expression of (2)

$$\theta_{approx}(y_0) = \frac{QV_0}{2E_k}\,\pi\ \text{erf}\left(\frac{y_0}{\Delta_r}\right) + C \qquad (4)$$

with the constant C = 0 since θ (0) = 0

We set the maximum deviation angle

$$\theta_{max} = \frac{QV_0}{2E_k} \cdot \pi \qquad (5)$$

and are thus in position to summarise

$$\theta_{approx}(y_0) = \theta_{max}\ \text{erf}\left(\frac{y_0}{\Delta_r}\right) \qquad (4)$$

$$\left(\frac{d\theta(y_0)}{dy_0}\right)_{approx} = \frac{2\theta_{max}}{\sqrt{\pi}\cdot\Delta_r}\ \exp\left(-\frac{y_0{}^2}{\Delta_r{}^2}\right) \qquad (3)$$

$$\Delta_r = \frac{2\theta_{max}}{\sqrt{\pi}} \quad \frac{1}{(d\theta/dy_0)|y_0 \to 0} \qquad (6)$$

D) Another expression of the transverse r.m.s value. Keeping the hypotheses of a Gaussian proton bunch
-n(r) is a 2-d Gaussian distribution ($r^2 = x^2 + y^2$) with r.m.s value Δ_r

- $\left(\frac{d\theta(y_0)}{dy_0}\right)_{approx}$ is a 1-d Gaussian distribution function of y_0 which r.m.s value

$$y_0, \text{ r.m.s} = \left[\frac{\int_{-\infty}^{\infty}\left(\frac{d\theta(y_0)}{dy_0}\right)_{approx} y_0^{\,2} dy_0}{\int_{-\infty}^{\infty}\left(\frac{d\theta(y_0)}{dy_0}\right)_{approx} dy_0}\right]^{1/2} = \frac{\Delta_r}{\sqrt{2}}$$

it is convenient to set

$$\sigma = \frac{\Delta_r}{\sqrt{2}} \qquad (7)$$

and to write instead

$$\theta_{approx}(y_0) = \theta_{max}\ \text{erf}\left(\frac{y_0}{\sqrt{2}\cdot\sigma}\right) \qquad (4)'$$

$$\left(\frac{d\theta(y_0)}{dy_0}\right)_{approx} = 2\,\theta_{max}\,\frac{1}{\sqrt{2\pi}\cdot\sigma}\exp\left(-\frac{y_0^{\,2}}{2\sigma^2}\right) \qquad (3)'$$

$$\sigma = \frac{1}{\sqrt{2\pi}}\,2\,\theta_{max}\,\frac{1}{(d\theta/dy_0)|y_0 \to 0} \qquad (6)'$$

APPENDIX 2

We aim to analyse in more detail the theoretical aspects of the shadow method.

As said the ion distribution on the observer plane is expressed by :

$$\frac{dn_i}{dY} = \frac{dn_i}{dy}\,\frac{dy}{dY} \qquad \text{A.2.1}$$

where $\frac{dn_i}{dy}$ is the curtain (or ion source) distribution measured when the proton beam is OFF.

We have :

$Y = y + L\,\theta\,(y) \equiv g\,(y)$ or $y = g^{-1}\,[Y]$

From 2 a,b : $\theta\,(y) = \theta_{max}\,\mathrm{erf}\left(\frac{y}{\Delta_r}\right)$, $\qquad \frac{d\theta(y)}{dy} = \frac{2\theta_{max}}{\sqrt{\pi}\cdot\Delta_r}\exp\left(\frac{y^2}{\Delta_r{}^2}\right)$

The function g(y) itself is not simple and therefore g^{-1} is not straightforward.

Since :

$$\frac{dg^{-1}}{dY}\,(Y) = \frac{1}{\frac{dg}{dy}\Big|y = g^{-1}(Y)}$$

and $\frac{dg}{dy}\,(y) = 1 + L\cdot\frac{2\theta_{max}(n_b)}{\sqrt{\pi}\cdot\Delta_r}\exp\left(-\frac{y^2}{\Delta_r{}^2}\right)$

we obtain :

$$\frac{dg^{-1}}{dY}(Y) = \frac{dy}{dY}\,(Y) = \frac{1}{1 + L\cdot\frac{2\theta_{max}(n_b)}{\sqrt{\pi}\cdot\Delta_r}\exp\left[-\left[\frac{g^{-1}(Y)}{\Delta_r}\right]^2\right]} \qquad \text{A.2.2}$$

remembering that θ_{max} depends on n_b and therefore on the proton beam intensity.

To illustrate this effect let us simplify and consider instead of an erf function a simplified expression :

$$\theta(y) = \begin{cases} \theta_{max}(n_b) \cdot \dfrac{y}{\Delta_r} & for\ |y| \le 2\Delta_r \\ \theta_{max}(n_b) & for\ |y| > 2\Delta_r \end{cases}$$

$$g(y) = Y(y) = \begin{cases} y + L \cdot \theta_{max}(n_b) \cdot \dfrac{y}{\Delta_r} & for\ |y| \le 2\Delta_r \\ y + L \cdot \theta_{max}(n_b) & for\ |y| > 2\Delta_r \end{cases}$$

$$g^{-1}(Y) = y(Y) = \begin{cases} \dfrac{Y}{1 + L \cdot \dfrac{\theta_{max}(n_b)}{\Delta_r}} & for\ |Y| \le 2\Delta_r + L \cdot \theta_{max}(n_b) \\ Y - L \cdot \theta_{max}(nb) & for\ |Y| > 2\Delta_r + L \cdot \theta_{max}(n_b) \end{cases}$$

Then we have :

$$\frac{dn_i}{dY} = \frac{dn_i}{dy} \begin{cases} \dfrac{1}{1 + L \cdot \dfrac{\theta_{max}(n_b)}{\Delta_r}} & for\ |Y| \le 2\Delta_r + L \cdot \theta_{max}(n_b) \\ 1 & for\ |Y| > 2\Delta_r + L \cdot \theta_{max}(n_b) \end{cases}$$

Fig. A.2.1 shows the curves $\frac{dn_i}{dY}$ as a function of Y for $\Delta_r = 10^{-3}$m , L = 0.5 m and for two different values of θ_{max} , namely for $\theta_{max} = 5\times10^{-3}$ rad (curve dni1/dY)) and for $\theta_{max} = 10\times10^{-3}$ rad (curve dni2/dY) .We considered only the simple case in which the initial ion curtain distribution is uniform, that is $\frac{dn_i}{dy}$ = const. (we took $\frac{dn_i}{dy} = 1$) .

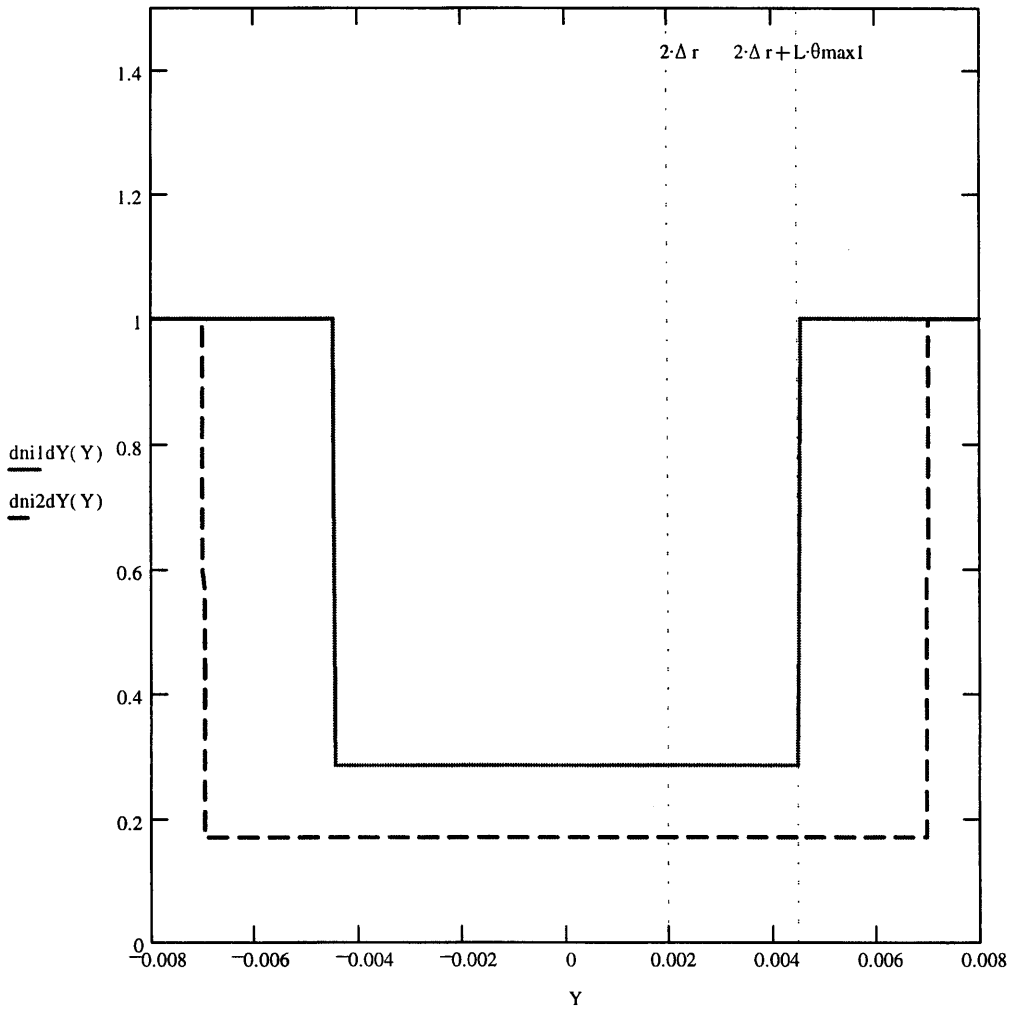

Figure A.2.1

We see that the deflation width on the phosphor screen is : $2\,(2\Delta_r + L\,\theta_{max}(n_b))$. The discontinuity of the curve occurs at $Y = (2\,\Delta_r + L\,\theta max\,(n_b))$ and will remain at this point if Δ_r and θ_{max} both vary in such a way that $d(Y) = d\,(2\,\Delta_r + L\,\theta_{max}(n_b)) = 0$ or $2\,d(\Delta_r) = L\,d(\theta_{max}(n_b))$ i.e. the r.m.s proton beam size variation $d(\Delta_r)$ is compensated by a variation of θ_{max} due to an increase of bunch intensity (n_b) and vice versa.

APPENDIX 3

We have seen that the Xe^+ beam coming out of the source has a conical distribution . This ion beam is collimated, steered and focused in order to obtain the ion curtain. (Fig. 5) Therefore, not only do the probe ions move in the x direction but they also have a velocity component lying in the yz plane.

Figure A.3.1 shows the projection of the probe ion trajectory in the xy plane and Figure A.3.2 shows the projection of the probe ion trajectory in the xz plane. The parameters D=916 mm and L=395 mm are given in Fig. 5 .

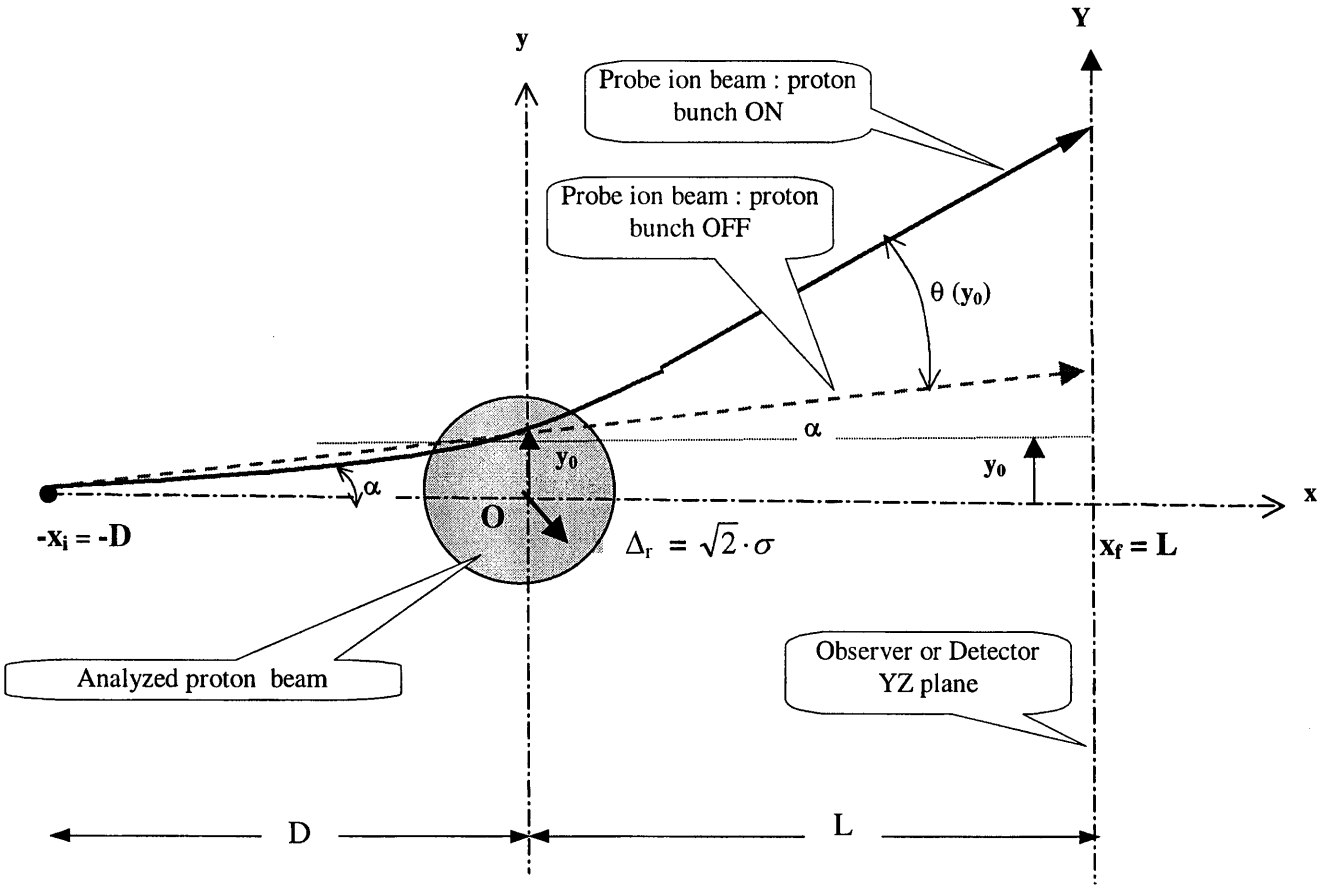

Figure A.3.1

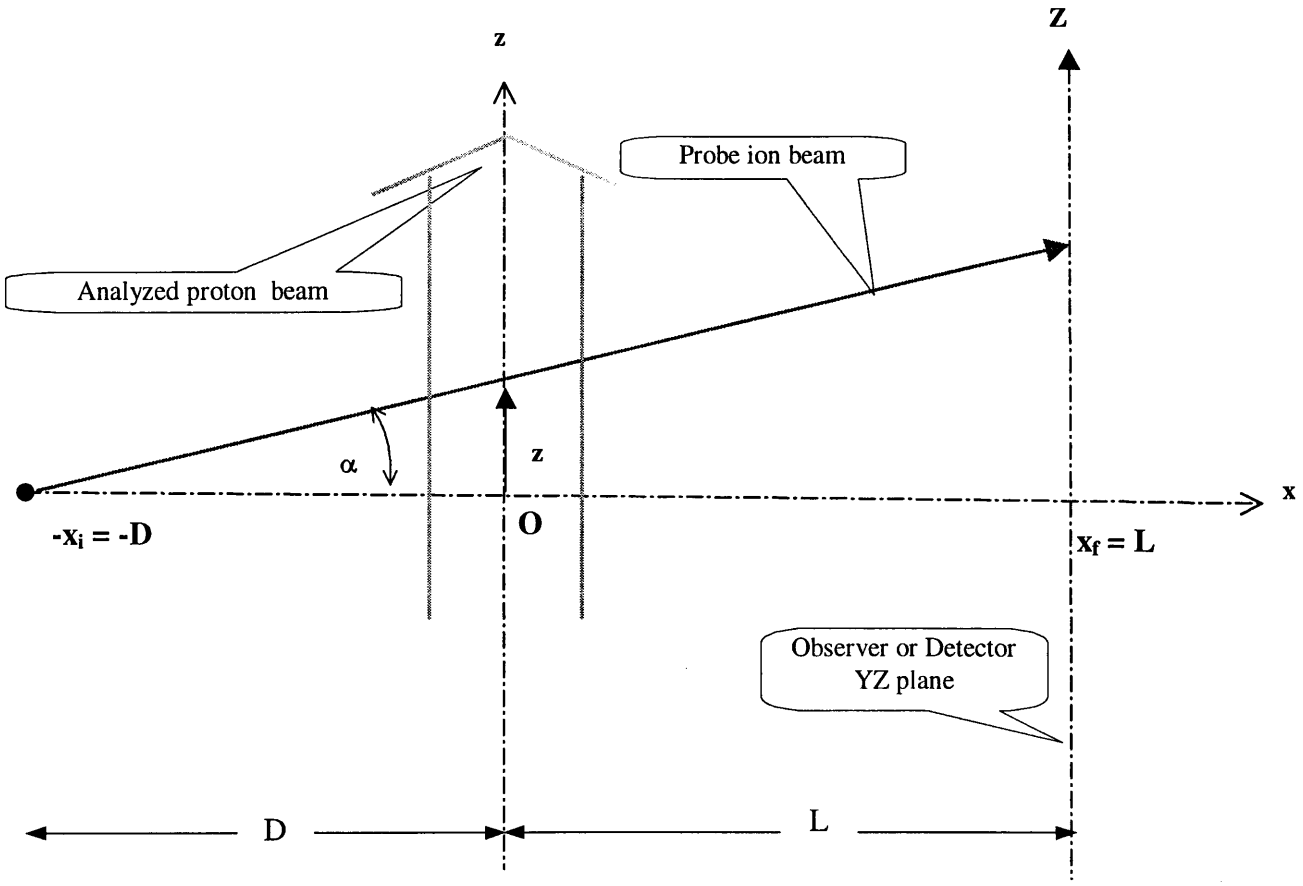

Figure A.3.2

With the proton-bunch OFF the probe ion reaches the observer plane (Fig. A.3.1) at $Y = (L+D)\cdot tg\alpha \cong (L+D)\cdot \frac{y_0}{D} = (1+\frac{L}{D})\cdot y_0$ whereas with the proton-bunch ON the probe ion is also deflected by an angle $\theta(y_0)$ and hence reaches the observer plane at $Y = (1+\frac{L}{D})\cdot y_0 + L\cdot tg\theta(y_0) = (1+\frac{L}{D})\cdot y_0 + L\cdot\theta(y_0)$.

In both cases the probe ion drifts in the z direction (Fig. A.3.2) and reaches the observer plane at $Z = (1+\frac{L}{D})\cdot z$.

This geometrical set-up was actually taken into account in the treatment of experimental data. However, in order to simplify the notations, we considered throughout the paper the ion source to be very far away from the probed beam ($D \to \infty$) so that the y,z velocity components of the ions are practically negligible and $1+\frac{L}{D} \cong 1$.

DISTRIBUTION :

ARDUINI Gianluigi	SL-OP	Z09600
BAL Cathelijne	PS-BD	L03200
BELLEMAN Jeroen	PS-BD	G03010
BENEDIKT Michaël	PS-OP	L04200
BOSSER Jacques	PS-BD	L07210
BOVET Claude	SL-BI	Y03410
BRAUN Hans-Heinrich	PS-LP	L19810
CASPERS Friedhelm	PS-RF	G02200
CHANEL Michel	PS-CA	L07300
CHEVALLAY Eric	PS-OP	L05410
COLLINS Ian	LHC-VAC	M28400
DEHNING Bernd	SL-BI	Y02500
DIMOPOULOU Christina	PS-BD	L07810
FERIOLI Gianfranco	SL-BI	Z13810
FISCHER Claude	SL-BI	Z13710
GIOVANNOZZI Massimo	PS-CA	G01200
GONZALEZ Jose-Luis	PS-BD	G02810
GOURBER-PACE Marine	PS-OP	L04710
GROBNER Oswald	LHC-VAC	M28800
HANKE Klaus	PS-HP	L04120
HILL Charles	PS-HP	L03510
JUNG Roland	SL-BI	Z13500
KEIL Eberhard	SL-AP	M08310
KOZIOL Héribert	PS-BD	L08910
KUCHLER Detlef	PS-HP	L03720
KUGLER Hartmut	PS-HP	L20810
LEBRUN Philippe	LHC	M21510
LINNECAR Trevor	SL-HRF	Z01600
MACCAFERRI Remo	PS-BD	L07510
MOLINARI Gianni	PS-BD	L07600
ODIER Patrick	PS-BD	G02900
PRIETO Virginia	PS-BD	L07200
RIEGE Hans	LHC-DLO	E08100
SCHMICKLER Hermann	SL-BI	Y01500
SCHMIDT Rudiger	LHC-ICP	M26620
STEINBACH Charles	PS-OP	L06600
TRANQUILLE Gérard	PS-OP	L06520
WILDNER Elena	SL-AP	M08600